5. R. J. Phillips, M. J. Shane, J. A. Switzer, *J. Mater. Res.* **4**, 923 (1989).
6. J. A. Switzer, *Am. Ceram. Soc. Bull.* **66**, 1521 (1987).
7. ———, *J. Electrochem. Soc.* **133**, 722 (1986).
8. ———, U.S. Patents, 4,492,811; 4,495,046; 4,521,499; 4,592,807; 4,626,322; and 4,608,750.
9. W. Mindt, *J. Electrochem. Soc.* **116**, 1076 (1969).
10. A. C. Ramamurthy and T. Kuwana, *J. Electroanal. Chem.* **135**, 243 (1982).
11. J. C. G. Thanos and D. W. Wabner, *ibid.* **182**, 25 (1985).
12. M. Sakai, T. Sekine, Y. Yamazaki, *J. Electrochem. Soc.* **130**, 1631 (1983).
13. W. Tillmetz and D. W. Wabner, *Z. Naturforsch. Teil B* **39**, 594 (1984).
14. A. Brenner, *Electrodeposition of Alloys* (Academic Press, New York, 1963), vol. 2, p. 589.
15. U. Cohen, F. B. Koch, R. Sard, *J. Electrochem. Soc.* **130**, 1987 (1983).
16. D. Tench and J. White, *Metall. Trans. A* **15**, 2039 (1984).
17. C. Ogden, *Plat. Surf. Finish.* **5**, 133 (1986).
18. J. Yahalom and O. Zadok, *J. Mater. Sci.* **22**, 499 (1987).
19. D. S. Lashmore and M. P. Dariel, *J. Electrochem. Soc.* **135**, 1218 (1988).
20. J. Yahalom *et al.*, *J. Mater. Res.* **4**, 755 (1989).
21. A. R. Despic, V. D. Jovic, S. Spaic, *J. Electrochem. Soc.* **136**, 1651 (1989).
22. T. W. Barbee, F. Spaepen, L. Greer, Eds., *Multilayers: Synthesis, Properties and Non-Electronic Applications* (Materials Research Society Symposium Proceedings 103, Materials Research Society, Pittsburgh, PA, 1988).
23. L. H. Bennett *et al.*, *J. Magn. Magn. Mater.* **67**, 239 (1987).
24. U. Atzmony, L. J. Swartzendruber *et al.*, *ibid.* **69**, 237 (1987).
25. V. N. Shukla and G. P. Wirtz, *J. Am. Ceram. Soc.* **60**, 253 (1977).
26. P. T. Moseley, J. L. Hutchison, M. A. M. Bourke, *J. Electrochem. Soc.* **129**, 876 (1982).
27. Y. Syono and S. Akimoto, *Mater. Res. Bull.* **3**, 153 (1968).
28. H. E. Cook and J. E. Hilliard, *J. Appl. Phys.* **40**, 2191 (1969).
29. A. Segmuller, P. Krishna, L. Esaki, *J. Appl. Crystallogr.* **10**, 1 (1977).
30. I. K. Schuller and C. M. Falco, *Surface Sci.* **113**, 443 (1982).
31. For a review of high-temperature superconductors, see A. W. Sleight, *Science* **242**, 1519 (1988).
32. One of the authors (J.A.S.) thanks Mitsubishi Corporation for financial support through a Mitsubishi Kasei faculty development award. We also thank Unocal Corporation for donation of all of the electrochemical instrumentation used in this research, and we thank G. McManus for assistance with x-ray diffraction and scanning electron microscopy.

28 August 1989; accepted 27 November 1989

Stratospheric Hydroperoxyl Measurements

WESLEY A. TRAUB, DAVID G. JOHNSON, KELLY V. CHANCE

The hydroperoxyl radical (HO_2) plays a key role in stratospheric chemistry through the HO_x catalytic cycle of ozone destruction. Earlier measurements of stratospheric HO_2 have given mixed results; some measured mixing ratios greatly exceed theoretical predictions. Measurements of HO_2 have now been made with a balloon-borne far-infrared spectrometer. The measured daytime profile is in excellent agreement with theory up to 40 kilometers; above this level the measurements exceed theory by 30 percent, perhaps because of underprediction of ozone at these altitudes. The nighttime HO_2 profile is strongly depressed with respect to the daytime profile, in general agreement with theory.

IN THE MIDDLE STRATOSPHERE (*1*), HO_x chemistry is driven by excited atomic oxygen, $O(^1D)$, which is produced by solar ultraviolet (UV) photolysis of ozone (O_3). The $O(^1D)$ reacts with water vapor to create OH, which in turn reacts with O_3 to yield HO_2, the hydroperoxyl radical. Together HO_2 and OH then catalytically destroy O_3 and O. It is believed that HO_x reactions are responsible for ~90% of the total O_3 and O losses at 60 km, but only ~10% at 40 km and below (*2*). The HO_x reactions also provide important production and loss terms in the chemistry of active Cl and N species.

The full atmospheric chemistry of HO_2 is relatively complex and includes at least three production and seven loss reactions, not all of which have well-understood reaction rates (*2, 3*). However, in a simplified picture, the strong attenuation of solar UV with depth in the stratosphere suggests that daytime HO_2 will be relatively more abundant above the ozone layer (~35 km) than below. At night, the concentration of HO_2 plummets because of loss reactions and the absence of UV light; the largest relative change occurs in the lower stratosphere, where loss reactions are most rapid.

Theoretical models of stratospheric chemistry are widely used to predict future response of the ozone layer to both natural and anthropogenic changes. The veracity of these predictions depends upon the accuracy and completeness of the models. Clearly, one way to verify the models is to see if they concur with measurements of the present stratosphere. For the case of HO_2, three types of measurements have been reported: two in situ methods [resonance fluorescence (*4*) and matrix isolation (*5*)] and a ground-based method [millimeter-wave (*6*)]. In a recent assessment (*2*) of theory and observation, the in situ measurements of HO_2 were found to be high with respect to current theory, but the ground-based measurements were in agreement; as a result, if the in situ observations are correct, then substantial changes would be required in our understanding of both HO_x chemistry and the ozone budget.

We have measured HO_2 with a far-infrared spectrometer (FIRS-2) that was mounted on a balloon-borne platform and viewed the atmosphere above the earth's limb through a small telescope (*7, 8*). The FIRS-2 had an effective spectral resolution of 0.008 cm^{-1} over the range 80 to 250 cm^{-1}. This region includes many molecular rotational lines that are thermally populated at stratospheric temperatures (*9*). Because the earth's troposphere is essentially opaque in

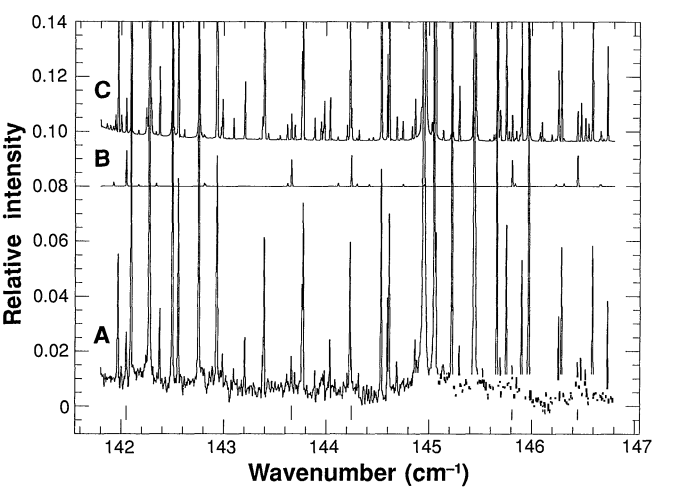

Fig. 1. (**A**) Measured daytime stratospheric spectrum from 142 to 147 cm^{-1} (see text). The intensity is normalized to a 277-K blackbody. (**B**) Theoretical spectrum showing only HO_2, vertically offset by +0.08 for clarity. (**C**) Theoretical spectrum including all species, also offset by +0.08 [the apparent baseline difference between (B) and (C) is caused by an empirically determined continuum component in our model; the physical origin of this continuum is thought to be the far wings of water vapor lines]. Tic marks at bottom show the five HO_2 lines used in our analysis.

Harvard-Smithsonian Center for Astrophysics, 60 Garden Street, Cambridge, MA 02138.

the far infrared and because the viewing geometry is especially favorable when the observing platform is above the altitude of the regions of interest, a balloon or satellite platform is required for stratospheric measurements.

Data were obtained during the second flight of the FIRS-2 spectrometer, launched from Palestine, Texas (32°N), on 12 May 1988. Both the daytime and nighttime stratosphere were measured during a 17-hour period from an altitude of ~39.0 km. The gondola was oriented to give a north-looking azimuth (±2°) for constant local solar time (LST) along the line of sight. Spectra were measured at elevation angles from −4.62° to 30°, which correspond to effective sampling altitudes from 19 to 49 km. In order to maximize the signal-to-noise ratio of the data, the spectra were added in two groups, a 6-hour daytime series centered at about 15.0 LST, and a 6-hour nighttime series centered at about 0.0 LST. The integration time in the summed spectrum at each observation angle was about 0.8 hours for the daytime data and 0.6 hours for the nighttime data.

The far-infrared rotational spectrum of HO_2 comprises a large number of *b*-type rotational lines. The positions of the HO_2 lines are known to better than 0.001 cm^{-1} on the basis of millimeter-wave and far-infrared measurements; the strengths are accurately known from measurements of the *b*-type component of the dipole moment (*10*).

Using our −2.32° daytime spectrum, we located 31 identifiable *R* branch lines and *Q* branch features of HO_2 between 95 and 185 cm^{-1}. Of these, the most useful were *R* branch lines lying between 142 and 147 cm^{-1} (Fig. 1).

The HO_2 mixing ratio profiles were determined as follows. Starting with the 30° ray and working down, we compared a 0.040-cm^{-1} region around each line to a synthetic spectrum generated from a layered model atmosphere; the model HO_2 in the most sensitive layer for that ray was adjusted until the two spectra agreed in a least-squares sense. For each spectral line, this process produced an independent estimate of the HO_2 mixing ratio profile, plus an estimate of uncertainty from noise in the spectrum.

The mixing ratio profiles were combined in a weighted average profile, where the weights were the inverse squares of the uncertainties (*11–13*) (Table 1 and Fig. 2). The calculations were iterated several times; the results are independent of the initial model profile.

Theoretical day and night profiles were generated by averaging time-dependent theoretical profiles (*13*) for time intervals corresponding to the observations (Fig. 2). The daytime data are in excellent agreement with the theoretical model from 25 to 40 km.

From 40 to 50 km, we measured about 30 ± 9% more daytime HO_2 than predicted by the theoretical model. There are two possible explanations for this difference: (i) The uncertainties in reaction rates involving HO_x production and loss in the model are large enough to allow the predicted mixing ratio to shift by roughly ±50%; a positive shift of this amount would bring the model prediction in line with our data. (ii) It may be related to the well-known characteristic of chemical models to unpredict O_3 between 40 and 50 km (*1, 2*). As mentioned above, daytime HO_2 depends on the production of $O(^1D)$, which in turn comes from the action of sunlight on O_3; thus if O_3 is underpredicted in a model, then HO_2 may be underpredicted as well. The FIRS-2 measures O_3 and other species simultaneously with HO_2; at 40 km and above, our results as well as those of many other investigators [(*2*), p. 14 and pp. 420–429] show that the measured O_3 mixing ratio is typically 40% or more greater than predicted by theoretical models. Below 25 km, our HO_2 exceeds the model, but the difference is not significant in consideration of the above-mentioned uncertainties in the measurement and model.

Table 1. Measured HO_2 mixing ratios for daytime and nighttime. Entries are mean values and uncertainties are ±1 SD. Where the uncertainty exceeds the mean, the 1 SD upper limit is shown; z_{eff} is the effective altitude.

Layer	Daytime		Nighttime	
	z_{eff} (km)	HO_2	z_{eff} (km)	HO_2
1	49.0	$44.67 \pm 2.70 \times 10^{-11}$	49.4	$12.01 \pm 8.00 \times 10^{-11}$
2	40.4	$19.42 \pm 1.35 \times 10^{-11}$	40.7	$0.48 \pm 0.32 \times 10^{-11}$
3	35.1	$7.81 \pm 1.66 \times 10^{-11}$	35.4	$1.14 \pm 1.00 \times 10^{-11}$
4	31.0	$5.44 \pm 0.91 \times 10^{-11}$	31.4	$< 1.28 \times 10^{-11}$
5	27.0	$1.29 \pm 0.63 \times 10^{-11}$	27.4	$< 0.65 \times 10^{-11}$
6	23.0	$1.67 \pm 0.60 \times 10^{-11}$	23.3	$< 0.36 \times 10^{-11}$
7	19.0	$< 1.83 \times 10^{-11}$	19.4	$< 0.61 \times 10^{-11}$

No nighttime HO_2 was detected below 32 km (Fig. 2), where the measured amounts are all less than the uncertainties. The HO_2 measurement near 35 km is larger than expected, but at a low level of significance. The measured nighttime HO_2 between 40 and 50 km is in agreement with the predicted amount to within the measurement uncertainty. We conclude that the measured diurnal behavior of HO_2 is in general agreement with theory.

Three other methods have been employed to measure stratospheric HO_2:

1) In in situ chemical conversion resonance fluorescence (*4, 14*), a descending measurement pod has been used from which addition of NO to a passing parcel of air converts HO_2 and NO to OH and NO_2; the OH is detected by resonance fluorescence in the (0 - 0) band at 309 nm with an onboard microwave discharge lamp. For comparison with our data, we formed a weighted average of the measurements from three flights in 1977 (Fig. 3), using the given detection threshold for each measurement as an uncertainty factor and then choosing for the overall uncertainty the larger of (i) the uncertainty from weights or (ii) the weighted scatter; the data combination method is thus identical to that used for our own data. We multiplied the resulting profile by 0.94 to account for the relatively larger amount of HO_2 expected during the resonance fluo-

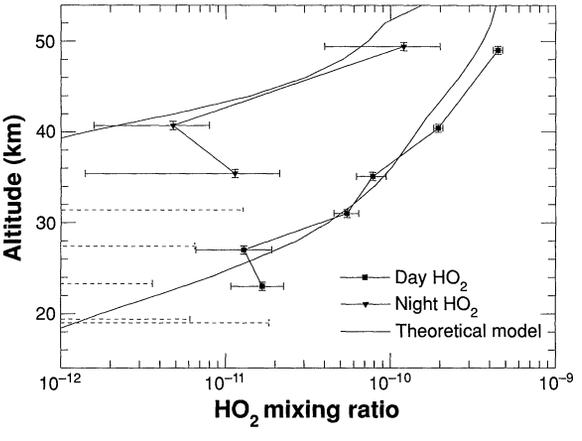

Fig. 2. Mixing ratio profiles of HO_2, from FIRS-2 measurements for daytime (15.0 LST; squares) and nighttime (0.0 LST; triangles); error bars indicate ±1σ. The corresponding model curves are time-averaged theoretical profiles (*13*). The uppermost two data points are tied together by an a priori ratio taken from the theoretical profile. Points at which only upper limits could be measured are indicated by dashed lines.

rescence measurements (effective solar zenith angle 46°) compared to our measurements (54°). The factor 0.94 is our estimate of the relative UV-induced difference in HO_2, near 33 km, between the two times and locales; it is based on the numerical change in HO_2 as the solar zenith angle is changed from 54° to 46° in our adopted theoretical model (*13*).

2) In matrix isolation and electron spin resonance (ESR) spectroscopy (*5, 15*), in situ samples have been captured in a water-ice matrix cooled with liquid He, returned to the laboratory, and analyzed by ESR to yield a composite HO_2-plus-RO_2 signature. We have converted the results of two flights in 1980 to mixing ratios, and scaled each value to correct for HO_2 variation with solar zenith angle, as above (Fig. 3).

3) In ground-based millimeter-wave spectroscopy (*6*), the stratospheric thermal emission spectrum near 265.8 GHz has been recorded from Mauna Kea, and three HO_2 rotational line profiles have been measured and compared with the expected line profiles from several different types of theoretical HO_2 mixing ratio distributions. This method is sensitive to the column abundance and broad shape of the HO_2 distribution in the upper stratosphere and lower mesosphere, but not to details of that distribution. The range of altitude sensitivity is bounded on the lower side by the point (~35 km) at which line broadening and the rapid drop-off in concentration cause the HO_2 features to become so wide (~40 MHz) and weak that they are masked by background noise. The bound on the upper side is where (~70 km) the line width drops below the resolution of the millimeter-wave filter bank (1 MHz) and altitude sensitivity is lost. Between these cutoff levels, the column integral reaches its 10 and 90% values at about 37 and 67 km, respectively. Within these adopted limits, the preferred millimeter-wave curve (*13*) gives an HO_2 column of 2.7×10^{13} cm^{-2}, which is ~1.25 times as large as the column integral from our theoretical curve. Both curves are similar in shape. To account for HO_2 variation with solar zenith angle (~43°), at a typical altitude (~46 km), we scaled by 0.94. The net result is that we can match the millimeter-wave results by scaling up our own theoretical profile by a factor of 1.18 (= 1.25 × 0.94) in the range 37 to 67 km (Fig. 3).

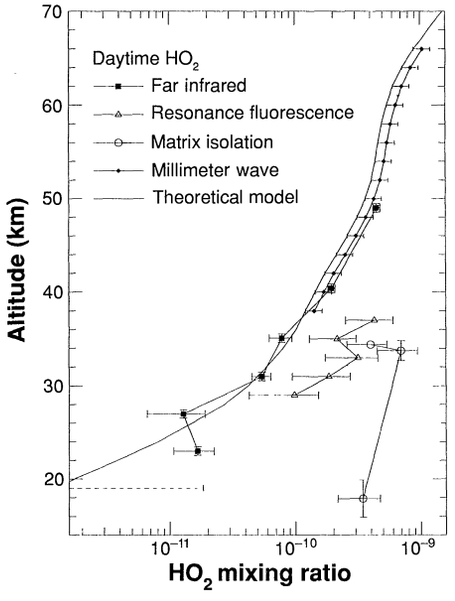

Fig. 3. The HO_2 daytime measurements (squares; Fig. 2), and other published HO_2 stratospheric data, averaged and scaled to remove the expected variation of HO_2 with solar zenith angle, as discussed in the text. The theoretical model is the same as in Fig. 2. All uncertainties are ±1σ. The in situ (open symbol) data points appear to be significantly biased with respect to both the present data and theory. As noted in the text, the present measurements, taken along with the millimeter-wave data (*6*), are in good general agreement with theory.

To the extent that the HO_2 mixing ratio is driven by the source chemistry factors of ozone, water, and UV flux and that the UV flux is removed by our scaling procedure, it follows that the four data sets (Fig. 3) should differ only insofar as the ozone and water are variable. The differences between the remote sensing and in situ methods are substantial: the resonance fluorescence profile is roughly four times as large as the theoretical profile, and the upper two matrix isolation points are about seven times as large; the matrix isolation point at 18 km shows an even larger difference. Because variations in O_3 and H_2O near 33 km altitude are probably limited to ~15% (*16, 17*), it is highly improbable that HO_2 could vary by the factor of 4 to 7 implied by the data (Fig. 3). Most likely the in situ methods are significantly biased toward high measurements.

The millimeter-wave data are in quite good agreement with our data, even though the two sets refer to different years and latitudes. Taken together, they are in agreement with the theoretical HO_2 profile over essentially the entire stratosphere and lower mesosphere.

REFERENCES AND NOTES

1. M. B. McElroy and R. J. Salawitch, *Science* **243**, 763 (1989).
2. Global Ozone Research and Monitoring Project, *Atmospheric Ozone 1985: Assessment of Our Understanding of the Processes Controlling Its Present Distribution and Change* (*Rep. No. 16*, World Meteorological Organization, Geneva, 1986).
3. G. Brasseur and S. Solomon, *Aeronomy of the Middle Atmosphere* (Reidel, Dordrecht, Holland, 1984).
4. J. G. Anderson, H. J. Grassl, R. E. Shetter, J. J. Margitan, *Geophys. Res. Lett.* **8**, 289 (1981).
5. M. Helten, W. Platz, M. Trainer, H. Fark, E. Klein, D. H. Ehhalt, *J. Atmos. Chem.* **2**, 191 (1984).
6. R. L. deZafra, A. Parrish, P. M. Solomon, J. W. Barrett, *J. Geophys. Res.* **89**, 1321 (1984). The uncertainty in the scale factor for this experiment is ±15%.
7. K. V. Chance, D. G. Johnson, W. A. Traub, *ibid.* **94**, 11059 (1989).
8. L. M. Coyle, G. Aurilio, J. Bortz, K. V. Chance, B. G. Nagy, G. U. Nystrom, W. A. Traub, *Rev. Sci. Instrum.* **57**, 2512 (1986); W. A. Traub, L. M. Coyle, K. V. Chance, *ibid.*, p. 2519 (1986).
9. W. A. Traub and M. T. Stier, *Appl. Opt.* **15**, 364 (1976),
10. H. M. Pickett, personal communication; S. Saito and C. Matsumura, *J. Mol. Spectrosc.* **80**, 34 (1980); selected HO_2 lines have recently been measured to a precision of $\sim 10^{-6}$ cm^{-1} with tunable far-infrared laser spectroscopy (K. V. Chance, K. M. Evenson, D. A. Jennings, M. D. Vanek, I. G. Nolt, K. Park, in preparation).
11. The average mixing ratios in the upper two layers were multiplied by 0.96 to allow for the model's increasing mixing ratio above ~50 km. The measured overhead column was distributed between the two upper layers in proportion to the ratio expected from our theoretical model [see text and (*13*)]; therefore, the derived mixing ratios in these layers are coupled.
12. The 1σ uncertainty in the mean mixing ratio was taken to be the quadrature sum of the following: (i) the larger of the inverse square root of the sum of the weights or the weighted rms scatter of data points about the mean; (ii) uncertainties from line strength (1.5%), intensity scale factor (1.0%), and atmospheric temperature (0.6%); and (iii) error propagated from upper to lower layers (3 to 17%).
13. M. A. Allen, personal communication; _____ and M. L. Delitsky, in preparation. The theoretical model was based on a one-dimensional, time-dependent, local photochemical calculation of the abundances of 7 atomic and 81 molecular species (of which 4 were preset: O_2, N_2, CH_4, and O_3) with 248 chemical reactions. Abundances were calculated from 16 to 100 km in steps of 2 km, for a 24-hour time period in 53 steps of 0.16 to 1.00 hours, and for the latitude and date of our flight. Chemical kinetic and photochemical data were from W. B. DeMore, M. J. Molina, S. P. Sander, D. M. Golden, R. F. Hampson, M. J. Kurylo, C. J. Howard, A. R. Ravishankara *NASA Publ. 87-41* (1987).
14. For the resonance-fluorescence method (*4*) at altitudes of 37, 35, 33, 31, and 29 km, we used the following: weighted mean mixing ratios at each altitude (4.54, 2.29, 3.42, 1.96, and 1.04) × 10^{-10}; HO_2 multiplier 0.94 (see text); and resulting mixing ratios (4.27 ± 1.67, 2.15 ± 0.94, 3.15 ± 1.19, 1.84 ± 0.88, and 0.98 ± 0.66) × 10^{-10}, respectively.
15. For the matrix isolation method (*5*) at altitudes of 34.4, 33.8 ± 1.1, and 17.9 ± 2.0 km, we used the average air density over the indicated altitude range to convert number densities to mixing ratios (D. H. Ehhalt, personal communication), with the following results: original mixing ratios at each altitude (3.32, 2.40, and 1.95) × 10^{-10}; HO_2 multipliers 1.20, 2.91, and 1.76; and resulting mixing ratios (3.98 ± 1.43, 6.98 ± 2.51, and 3.43 ± 1.27) × 10^{-10} respectively.
16. For ozone, the measured long-term (~6-year) trend at 33 km between 20°N and 50°N is roughly 0 ± 1%, with a possible additional 4% systematic uncertainty [(*17*), p. 55]; the monthly and yearly standard deviation for ozone at 33 km in the Northern Hemisphere is about 3% [(*2*), p. 417]; daily fluctuations have not been reported, but may be estimated to be ~10% [(*2*), p. 431]; on this basis, we take the total variation of O_3 at ~33 km to be under ~15%. For water vapor, no long-term trend has been measured, but an increase might be anticipated on the basis of the measured increase in tropospheric CH_4 (methane) of 1 to 2% per year, some of which will reach the stratosphere where it will oxidized to H_2O (*1, 2*); seasonal fluctuations of H_2O at 33 km and 32°N are measured to be about ±3% [(*2*), p. 466]; daily fluctuations of H_2O near 33 km are believed to be much less than ~30% [(*2*), p. 463]; therefore, we adopt an upper limit of ~15% for the total variation of H_2O at ~33 km.

17. *Present State of Knowledge of the Upper Atmosphere 1988: An Assessment Report* (*NASA Ref. Publ. 1208*, National Aeronautics and Space Administration, Washington, DC, 1988).
18. This work was supported by NASA grant NSG-5175, under the Upper Atmospheric Research Program. We thank the National Scientific Balloon Facility for balloon launch services, the Jet Propulsion Laboratory for gondola services, M. A. Allen for theoretical mixing ratio profiles, A. Ghosh for computational assistance, and R. L. deZafra, D. H. Ehhalt, and S. C. Wofsy for comments.

8 September 1989; accepted 14 November 1989

A Regulatory Gene as a Novel Visible Marker for Maize Transformation

STEVEN R. LUDWIG, BEN BOWEN, LARRY BEACH, SUSAN R. WESSLER*

The temporal and spatial patterns of anthocyanin pigmentation in the maize plant are determined by the presence or absence of the *R* protein product, a presumed transcriptional activator. At least 50 unique patterns of pigmentation, conditioned by members of the *R* gene family, have been described. In this study, microprojectiles were used to introduce into maize cells a vector containing the transcription unit from one of these genes (*Lc*) fused to a constitutive promoter. This chimeric gene induces cell autonomous pigmentation in tissues that are not normally pigmented by the *Lc* gene. As a reporter for gene expression studies in maize, *R* is unique because it can be quantified in living tissue simply by counting the number of pigmented cells following bombardment. *R* may also be useful as a visible marker for selecting stably transformed cell lineages that can give rise to transgenic plants.

MOST MAIZE CELL TYPES HAVE THE capacity to accumulate anthocyanin pigments (*1*). Pigmentation within the plant is controlled by at least ten genes that encode regulatory or structural proteins of the anthocyanin biosynthetic pathway (*2*). The *R* gene family determines the location, timing, and amount of anthocyanin expression in the maize plant and seed (*3*). The overall pigmentation pattern in the plant represents the additive effect of each family member.

The *R-Navajo* (*R-nj*) gene, which pigments the crown of the kernel, was cloned by tagging with the transposable element *Ac* (*4*) and was found to be homologous with three other *R* genes, *P*, *S*, and *Lc*, which display different pigmentation patterns (*4*). Homology between *R-nj* and *Lc* facilitated the cloning of a full-length *Lc* cDNA. The protein encoded by this cDNA has features characteristic of transcriptional activators and DNA binding proteins (*5*). From these data and previous genetic analyses (*6*), we proposed that the diverse patterns of anthocyanin pigmentation conditioned by different *R* genes reflect differences in the *R* gene promoters rather than their gene products (*5*).

To test this hypothesis, we used microprojectile bombardment (*7, 8*) in an in vivo assay to analyze *R* gene expression. We bombarded maize kernels with microprojectiles (*9*) coated with the vector pPHI443, which contains the entire *Lc* protein coding region fused to a constitutive promoter from cauliflower mosaic virus (*10*). Pigmented cells were detected in the aleurone layer 14 to 36 hours after bombardment (Fig. 1A). In the absence of pPHI443 DNA, aleurone cells were unpigmented because they lacked a functional *R* gene. Since the *Lc* gene does not normally pigment aleurone cells, this experiment supports our contention that *R* genes are functionally equivalent and that pigmentation can be induced in a novel tissue by changing the *R* promoter.

To examine the versatility of this marker, we bombarded a variety of tissues with pPHI443. After the bombardment of germinating seedlings, pigmented cells were seen in the epidermal cell layers of the coleoptile (Fig. 1B), primary root (Fig. 1C), mesocotyl, scutellar node, and coleorhiza (Fig. 1D). Pigmented cells were also observed in the surface cell layers of other immature tissues such as pericarp (both inner and outer layers), culm, husk, scutellum, and anther locules. In young leaves pigmentation was observed in both epidermal cells and trichomes (Fig. 1E).

To determine whether the introduced *R*-encoded protein is constrained by factors similar to those observed for endogenous *R* gene products, we cotransformed a variety of maize tissues with pPHI443 and an analogous vector, pPHI459, encoding β-D-glucuronidase (GUS) (*10*). Expression of both markers can be seen simultaneously in most tissues (Fig. 1F), because red cells retain their pigment when treated with GUS histochemical stain. However, in cells of the inner endosperm, pigmentation was never

S. R. Ludwig and S. R. Wessler, Botany Department, University of Georgia, Athens, GA 30602.
B. Bowen and L. Beach, Pioneer Hi-Bred International, Department of Biotechnology Research, Johnston, IA 50131.
S. R. Ludwig and B. Bowen should both be considered first authors as they contributed equally to this work.

*To whom correspondence should be addressed.

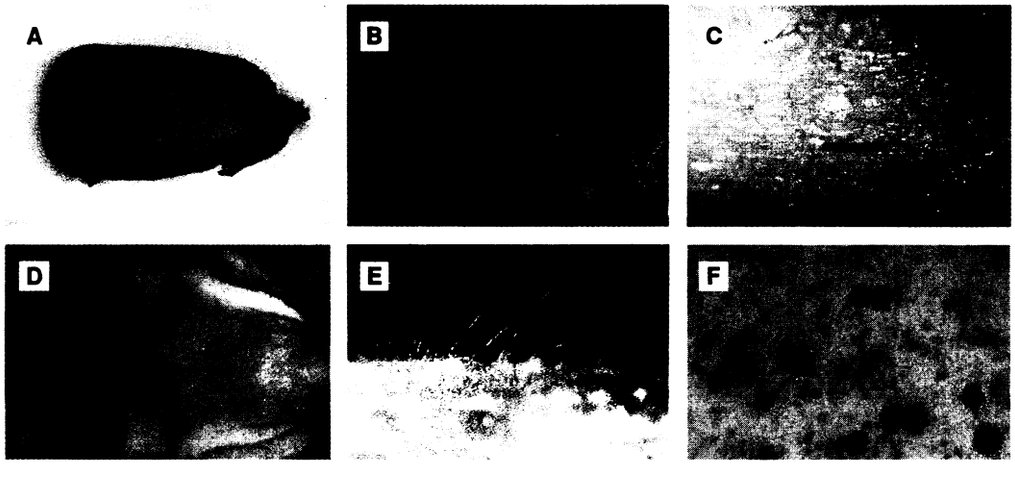

Fig. 1. Expression of an *R* gene introduced into different tissues. Aleurone (**A**), coleoptile (**B**), root (**C**), mesocotyl, scutellar node, coleorhiza (**D**), and marginal leaf hair (**E**) were bombarded with gold particles coated with pPHI443 DNA as described (*9*) and photographed approximately 48 hours later. Aleurone cells (**F**) cotransformed with pPHI443 and pPHI459 were examined after histochemical staining for GUS (*13*).